



Quantification of bottlenecks to fast charging of lithium-ion-insertion cells for electric vehicles



Rajeswari Chandrasekaran

Research and Advanced Engineering, Ford Motor Company, Dearborn, MI 48124, USA

HIGHLIGHTS

- Validated the lithium-ion cell sandwich model with experimental charge data.
- Quantified and analyzed the overpotential contributions at high charge rates.
- Magnitude of overpotentials increase with charge rate.
- Thermodynamic conditions favorable for lithium plating exist in the negative electrode from 2C charge rate.

ARTICLE INFO

Article history:

Received 16 May 2014

Received in revised form

15 July 2014

Accepted 16 July 2014

Available online 28 July 2014

Keywords:

Lithium-ion

Batteries

Fast charging

Electric vehicles

Modeling

Automotive

ABSTRACT

In this work, an isothermal, physics-based, dual lithium-ion insertion cell sandwich model is used for simulating the galvanostatic charge performance of a graphite (Li_xC_6)/liquid electrolyte/ $\text{Li}_y(\text{Ni}_a\text{Co}_b\text{Mn}_c)\text{O}_2$ at room temperature at various current densities. The modeling results are compared with experimental cell potential vs. capacity data. The validated model is used to identify the bottlenecks to fast charging by quantification of the various contributions to the cell overpotential. Lithium plating at the negative electrode is shown to be thermodynamically feasible during galvanostatic charging at 2C rate and above. This work will aid in research and development activities to overcome the hurdles to fast charging of advanced electric vehicle batteries.

© 2014 Elsevier B.V. All rights reserved.

1. Introduction

Vehicles with different levels of electrification are in the portfolio of most major automobile manufacturers to reduce tail pipe emissions, deliver higher fuel economy, and increase energy security by reducing dependence on foreign oil while delivering vehicles with good performance, durability, customer satisfaction and acceptable range [1]. Presently, the recharge time for battery electric vehicle (BEV) and plug-in hybrid electric vehicle (PHEV) is long compared to the refuel time for gasoline powered vehicles. For electric vehicles, the ability of a system to charge at high rates could be just as important as high-rate discharges [2] as it leads to increased customer acceptability by reducing range anxiety. Better fast charge acceptance also means improved ability to capture regenerative braking energy in hybrid electric vehicles. Charging at $\geq 2\text{C}$ rate or at even extreme rates of 10–20C rate should in

principle deliver a fully charged pack in 30 min and 6–3 min respectively. The US Department of Energy (DOE) has set a fast charge goal [3] of 10 miles of range per minute of fast charge. For an EV with 100 mile range (24 kWh battery pack), the DOE goal is to enable a full charge in 10 min (6C rate) and for a PHEV with 40 mile electric range (12 kWh battery pack) in 4 min (15C rate). If fast charging is such an important attribute, the question arises as to why fast charging is not widely available.

Researchers have been studying various methods to fast charge lithium-ion batteries, their effects on performance and capacity fade [4,5]. During charging, when a constant-voltage step is employed after a constant-current step, the total charging time initially decreases with increasing current [5]. It is not obvious how the total charging time will change with faster charge rates because of the various coupled phenomena occurring in the cell.

In one attempt to deliver a cell capable of fast potentiostatic charging, novel electrode architecture was reported in literature [6]. However, the capacity of the graphite negative electrode was

E-mail address: rchand35@ford.com.

designed to be ten times more than that of the positive electrode. This is not a practical ratio for lithium-ion cells for electric vehicles. Advances in positive electrode materials such as LiFePO₄ have been discussed in detail about their ability to sustain fast charging rates [7–9]. However, the weight percent of the conductive carbon was varied from 15% to 65% depending on the intended charge rate [7,9] and likewise impractical for automotive batteries. Several bottlenecks can limit the charge acceptance of an electric vehicle battery pack at high rates. Limitations to charging the coke/plasticized electrolyte/spinel sandwich up to 1.3C rate is available in literature [2]. In an earlier work, [1] the overpotentials arising from various mechanisms were systematically quantified and analyzed to identify the bottlenecks or limitations during fast charging (at 3C and 10C rate) of the coke/liquid electrolyte/spinel lithium-ion cell sandwich [10] from simulations. However, presently most lithium-ion cells employ a graphite based negative electrode with a positive insertion electrode and the electrodes are relatively thinner (and sometimes less porous) than before [11]. Therefore, it is worthwhile to analyze the bottlenecks to fast charging in these systems which are more representative of the current state of the art to better understand the origin of their limitations and possible approaches to improvement.

Quantification of contributions to cell overpotential during galvanostatic discharge of a graphite(Li_xC₆)/liquid electrolyte/Li_y(-Ni_aCo_bMn_c)O₂ cell sandwich were carried out recently [12] using an experimentally [11] validated physics-based model. However, it is imperative to analyze the bottlenecks to fast charge acceptance separately because: (a) the upper cut-off potential is closer to the thermodynamic open-circuit potential of the cell than the lower cut-off potential and therefore the rate capability effects may be more pronounced during charge than discharge of a dual lithium-ion insertion cell, contributing to the asymmetry in the obtained capacities [2], and (b) limitations to fast charging (and the asymmetry between charge and discharge capacity especially at high rates) can be due to the low thermodynamic open-circuit potential of the carbon based negative electrodes (such as graphite [13] or coke [10] in some cases) at high lithium content as this can lead to lithium plating under significant overpotential.

Therefore, the isothermal physics-based model [12] of the graphite (Li_xC₆)/liquid electrolyte/Li_y(Ni_aCo_bMn_c)O₂ cell sandwich was validated with experimental cell potential vs. capacity data during galvanostatic charging at various current densities or rates [14] at room temperature. In the present work the contributions to cell overpotential during galvanostatic fast charge of these advanced lithium-ion cells are quantified and analyzed from simulations with the validated model. Furthermore, thermodynamic insight into the possibility of lithium plating on the negative electrode is also provided. Modeling is an important tool for this research because experimentally measuring the various spatial temporal contributions to cell overpotential that limit the charging process is often difficult or impossible. The knowledge gained from this work will help in research and development activities to overcome fast charging issues in advance electric vehicles.

2. Modeling

The galvanostatic charge of Li_xC₆/liquid electrolyte/Li_y(Ni_aCo_bMn_c)O₂, i.e. dual lithium-ion insertion cell sandwich is modeled using macro-homogenous approach and concentrated solution theory. The underlying theories and equations have been discussed extensively in the past for similar systems [10], [15] and are therefore not repeated here. Although the liquid electrolyte in the experiments is LiPF₆ in EC:EMC:DMC in the ratio 3:4:3 with additives [11], for modeling purposes, the liquid phase is considered to be made up of binary electrolyte and a solvent. The thermodynamic

open-circuit potential vs. composition curves for the individual electrodes, ionic conductivity of the electrolyte as a function of salt concentration and the experimental charge curves are taken from prior work [11,14]. The experimental galvanostatic charge curves (cell capacity vs. voltage plots) [14] were obtained at 25 °C using an 18650 surrogate cell format with a designed capacity of 230 mAh (21.30 A m⁻² is the ideal 1C-rate) [11]. In the experiments [14], the cells were galvanostatically discharged at 0.5C rate and a rest period of one hour between the discharge and charge steps was provided. Although cell overpotential of 50 mV is associated with 0.5C rate discharge [12], the relaxation step should help avoid any confounding effects on the subsequent charge step.

Other parameters [11,12,14] are provided in Table 1. The sign of the applied current is negative for charging direction by convention in the simulations. The initial solid lithium concentrations of the individual electrodes for charge are, as expected, different from that for the discharge. The kinetic rate constants have to be slightly decreased at higher charge rates (2C and 3C rates) as seen in Table 1 for a better fit with the experimental curves [14]. The uncertainty in solid lithium concentration at the beginning of charge due to the difficulty in measuring them accurately justifies adjusting this parameter slightly as shown in Table 1 [14] for the positive electrode for a better fit at 3C charge rate.

The simulations of the coupled, transient, partial differential equations at all galvanostatic charge rates are carried out at 298 K, to the cell cut-off potential of 4.2 V (as in experiments) using COMSOL multiphysics finite element software (version 4.3). The

Table 1
Model input parameters.

Parameter description	Value
Constant-current density at 1C charge rate	-21.3 A m ⁻²
Radius of the secondary particle of the negative electrode active material	6.35 μm
C-rates at which the cell is charged	0.5; 1; 2; 3
Radius of the secondary particle of the positive electrode active material	5.15 μm
Transference number	0.363
Salt diffusion coefficient	7 × 10 ⁻¹¹ m ² s ⁻¹
Active material volume fraction in the positive electrode	0.62
Electrolyte volume fraction in the positive electrode	0.29
Bulk solid matrix electronic conductivity (positive)	0.5121 S m ⁻¹
Bulk solid matrix electronic conductivity (negative)	4.3317 S m ⁻¹
Initial electrolyte concentration	1300 mol m ⁻³
Active material volume fraction in the negative	0.65
Electrolyte (pore) volume fraction in the negative	0.33
Maximum solid phase lithium concentration (negative)	30,813 mol m ⁻³
Maximum solid phase lithium concentration (positive)	51,000 mol m ⁻³
Initial solid phase lithium concentration (negative)	1462.1 mol m ⁻³
Initial solid phase lithium concentration (positive)	35700 mol m ⁻³
0.5C–2C rate	36,720 mol m ⁻³
3C rate	1 × 10 ⁻¹¹ m s ⁻¹
Kinetic rate constant (negative)	0.5C and 1C rate
2C rate	0.6 × 10 ⁻¹¹ m s ⁻¹
3C rate	0.4 × 10 ⁻¹¹ m s ⁻¹
Kinetic rate constant (positive)	0.5C and 1C rate
2C rate	1 × 10 ⁻¹¹ m s ⁻¹
3C rate	0.6 × 10 ⁻¹¹ m s ⁻¹
Anodic and cathodic transfer coefficients	0.4 × 10 ⁻¹¹ m s ⁻¹
in the positive and negative electrodes	0.5
Geometric cross-sectional area of the cell	0.0108 m ²
Thickness of graphite (negative porous insertion electrode)	59.1 μm
Solid phase lithium diffusivity in negative particle	2 × 10 ⁻¹⁴ m ² s ⁻¹
Solid phase lithium diffusivity in positive particle	7.49 × 10 ⁻¹³ m ² s ⁻¹
Thickness of the separator	21 μm
Thickness of Li _y (Ni _a Co _b Mn _c)O ₂ (positive porous insertion electrode)	50 μm
Separator porosity	0.48
Bruggeman exponent in separator	3

time at which the cut-off potential is reached at a galvanostatic current density is considered the end of charge at that rate. Constant-voltage charging step is not used in this work. The electrolyte phase potential is arbitrarily defined to be zero at the positive-electrode/current-collector boundary. Time dependent, non-linear solver is used. Backward differentiation formula is used for time stepping.

Model coupling operators such as ‘integration’, ‘linear extrusion’ and ‘average’ are defined in domains or boundaries of interest in COMSOL and are called upon during post-processing to obtain the various overpotentials using corresponding expressions in the cell sandwich model. The charge transfer overpotentials are obtained from the kinetic rate equations at the respective electrodes. The variation of potential in the liquid electrolyte phase is given by a modified Ohm’s law [2,10] which has two terms: one is related to the ionic conductivity as expected and the other is related to the salt concentration variations.

3. Results and discussions

The comparison between experimental data and model predictions [14] are provided in Fig. 1 and a good fit is obtained. At the end of charging at 3C galvanostatic rate, only 71% of the low-rate (0.5C) charge capacity is obtained. The thermodynamic open-circuit potential curve of the cell in Fig. 1 is calculated for an initial solid lithium concentration of $35,700 \text{ mol m}^{-3}$ and $1462.1 \text{ mol m}^{-3}$ at the positive and negative electrodes respectively. Time (in seconds) is rounded off to the nearest whole number in the legend in the figures and in the discussion for convenience.

3.1. Contributions to cell overpotential from simulations

Cell overpotential is the difference between the thermodynamic open-circuit potential of the cell and the simulated cell potential. Cell potential is the difference between the solid phase potential of the positive and negative electrodes at the corresponding current collector/electrode boundaries. Fig. 2 gives the cell overpotential at all charge rates from simulation results and as expected, the overpotential is higher at higher rates of charge. The cell overpotential at the end of charging at 2C constant current density is 279 mV and the capacity reached is 154 mAh (i.e. 67% of its designed discharge capacity of 230 mAh). At a 3C galvanostatic rate, the cell can only be charged to 130 mAh (56.5% of its designed discharge capacity of

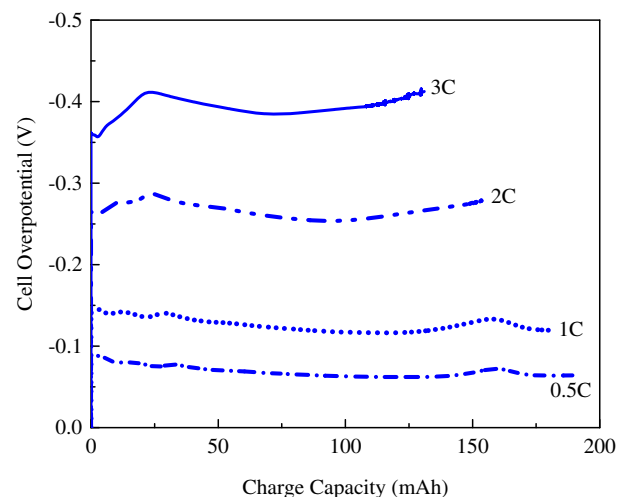


Fig. 2. Cell overpotential vs. charge capacity from simulations.

230 mAh) before the cut-off potential is reached due to a cell overpotential of 414 mV. In comparison, the cell delivered a galvanostatic discharge capacity of 190 mAh at the end of 3C rate with overpotential of 440 mV [12]. This confirms the asymmetry mentioned in the introduction section between charging and discharging directions and hence the need for the present study.

3.1.1. Potential for lithium plating during fast charge

Before investigating the contributions to cell overpotential in detail, it is useful to check if lithium plating will be thermodynamically favored at the negative electrode during charging in this system. If the difference between the solid phase and liquid phase potentials in the negative electrode reaches zero, lithium plating reaction becomes thermodynamically favorable. This potential difference reaches 0 V at the negative-electrode/sePARATOR boundary at approximately 501 s from the start of charging at 2C rate as seen in Fig. 3(a). At the end of charge at 2C rate (i.e. at 1202 s), this potential difference reaches 0 V and -35 mV at the current-collector/negative-electrode and the negative-electrode/sePARATOR boundaries respectively. This implies that if plating of lithium were to occur, it would start at the negative-electrode/sePARATOR boundary. This spatial variation at any given time is due to non-uniform current distributions across the negative electrode in the cell sandwich as will be discussed later. Fig. 3(b) shows that at a 3C rate, this electrode/electrolyte potential difference reaches 0 V at the negative-electrode/sePARATOR boundary at only 68 s from the beginning of charging and at the current-collector/negative-electrode boundary at 201 s. At the end of charging, this difference is approximately -100 mV at the negative-electrode/sePARATOR boundary. However, from simulations, it is found that this potential difference does not reach zero volts when the cell is charged at a constant current density of 21.3 A m^{-2} (1C rate). Whether lithium plating will actually occur depends on its kinetics relative to the main lithium insertion reaction and if the overpotential required for the nucleation step to form lithium metal is reached [2]. If lithium plating were to occur, the physics-based model has to be modified to include this side reaction and the performance predictions may accordingly change. This suggests that the uncertainty in model results is higher for 3C charge rate and so going forward, only results for 2C rate of charging will be discussed. It should be noted that if some of the limitations to fast charge are reduced or eliminated, then the risk of lithium plating can also decrease. Finally, during fast charging at 2C rate, the positive electrode potential difference between the solid and liquid

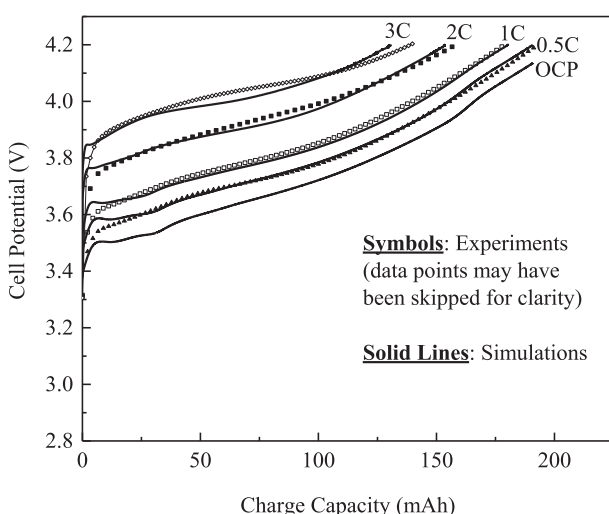


Fig. 1. Comparison between model predictions and experimental cell potential vs. capacity at various galvanostatic charge rates.

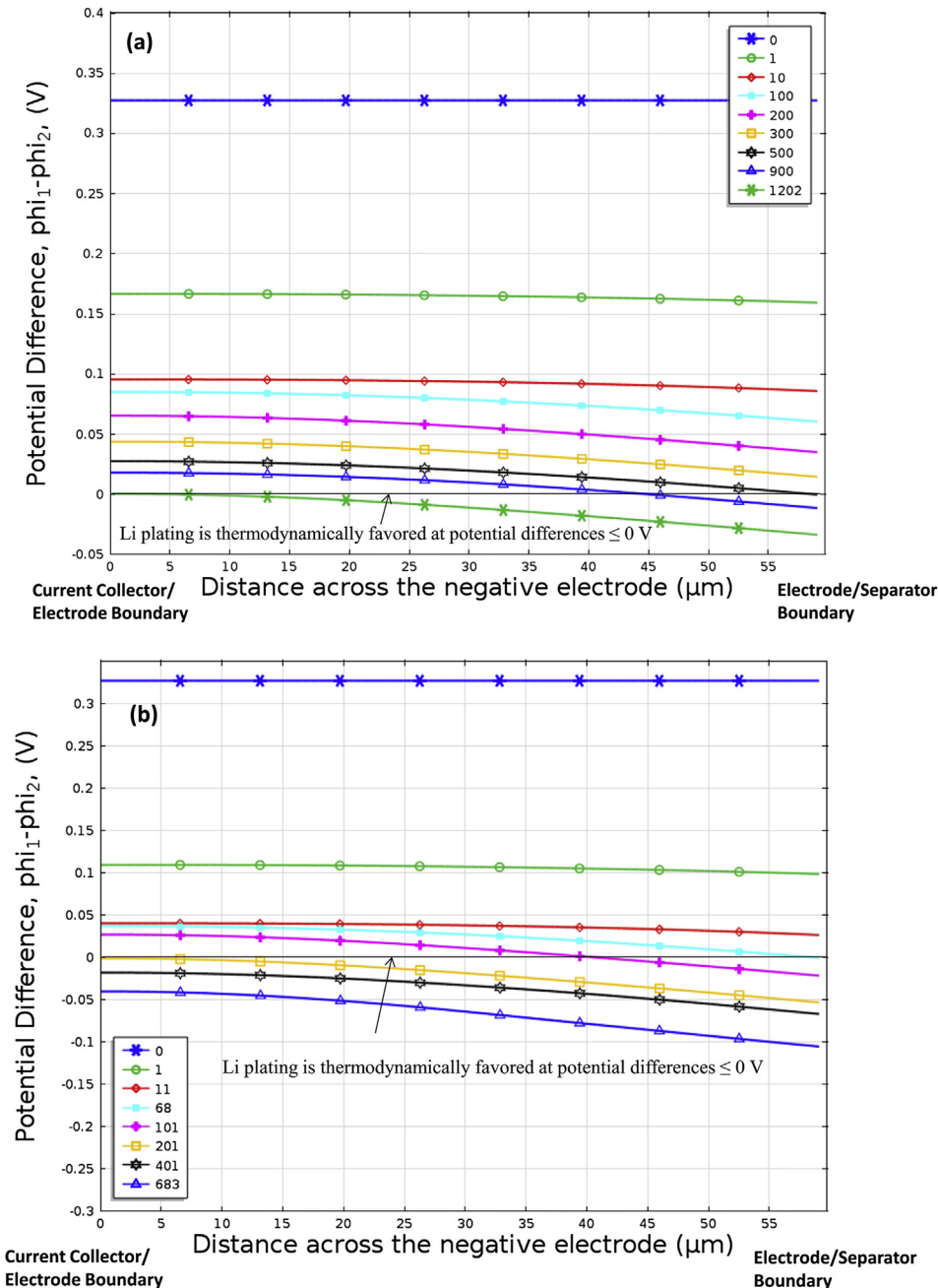


Fig. 3. (a) Potential difference between solid phase (ϕ_1) and liquid electrolyte phase (ϕ_2) in the negative electrode during galvanostatic charging at 42.6 A m^{-2} (2C rate). Legend is time in seconds from the start of the charge. (b) Potential difference between solid phase (ϕ_1) and liquid electrolyte (ϕ_2) phase in the negative electrode during galvanostatic charging at 63.9 A m^{-2} (3C rate). Legend is time in seconds from the start of the charge.

phase does not cross 4.15 V. Since this value is below the typical organic electrolyte decomposition threshold, overcharge [16] is not considered in this work.

3.1.2. Temporal variation of the potential losses at 2C charge rate

The various contributions to cell overpotential during galvanostatic charge at 2C rate are obtained from simulations and displayed in a stacked chart as a function of charge capacity in Fig. 4. The solid black curve is reproduced from Fig. 2. The individual contributions add up to the total cell overpotential (black curve) quite well for 2C rate. The reason for slight discrepancy could be that the charge transfer overpotential shown in Fig. 4 is obtained by taking average across the respective regions and not measured just at the terminals (i.e. current-collector/electrode boundaries). Fig. 4 shows that at a

2C charge rate, the charge transfer overpotentials in the electrodes (especially at the negative) dominate the cell overpotential.

In the simulated plots that are discussed below symbols are provided for clarity and do not represent actual experimental data or are not the only simulated data points. The numeric values in the legend in the simulated plots represent the time elapsed since the beginning of charge in seconds. In the discussion below, absolute values of overpotentials will be used for simplicity.

3.1.3. Ohmic overpotential

The ohmic drop due to electronic resistances in the composite electrodes is negligible and hence not seen in Fig. 4. The solid phase potential across each composite electrode is constant (hence figure not given) at any given time during the charge. However, if contact

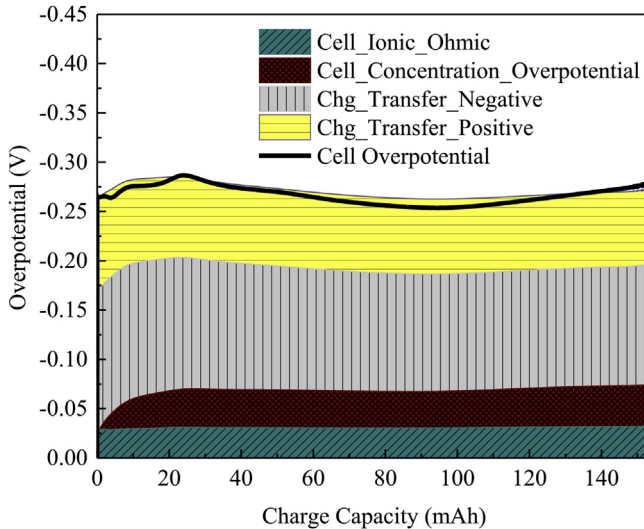


Fig. 4. Overpotential vs. charge capacity at 2C rate. Note: The simulated charge transfer overpotential at the positive electrode is multiplied by a negative sign for ease of stacking up in the above chart.

resistance is present, it can affect the electronic conductivity and influence the fit in Fig. 1 (especially at higher rates).

3.1.4. Ionic resistance and the ohmic drop in the electrolyte phase

Salt concentration varies with time and position in the cell sandwich during charge as shown in Fig. 5 at 2C rate (42.6 A m^{-2}). Fig. 4 shows that the total ohmic overpotential due to ionic resistance in the liquid electrolyte phase contributes 32 mV. Fig. 6 gives the contribution from each region of the cell to the total ionic ohmic drop during charging at 2C rate. The relative contributions are influenced by the magnitude of ionic current, void volume fraction (and tortuosity), salt concentration (Fig. 5), bulk ionic conductivity and the thickness of each region. The ohmic potential drop in the electrolyte phase is slightly higher in the positive electrode than in the negative electrode. The initial increase in the ionic ohmic drop in the

electrolyte phase in the positive electrode is followed by a constant value which is consistent with the quasi-steady state (discussed later) in the salt concentration profile in Fig. 5 from 150 to 300 s.

3.1.5. Total electrolyte phase potential drop

Fig. 7 provides the total liquid electrolyte phase potential across the cell sandwich during charging at 42.6 A m^{-2} (2C rate). The overpotential due to ionic resistance and the salt concentration overpotential from all three regions of the cell contribute to the total electrolyte phase potential drop. The electrolyte phase potential drop across the whole cell at 2C charge rate is roughly 75 mV towards the end of charge (Figs. 4 and 7 and Fig. A-1 for clarity) and the salt concentration overpotential increases from zero at the beginning of charge to roughly 43 mV. Thus, ohmic potential drop and salt concentration overpotential contribute 43% and 57% respectively to the total liquid phase potential drop at the end of 2C charge rate. The contribution to the total liquid phase electrolyte potential drop from the various regions of the cell during galvanostatic charging at 2C rate is given in Fig. 8. The negative electrode contributes the most at 2C rate. The salt concentration overpotential and the electrolyte phase potential drop attain almost a quasi-steady state around 150–300 s in Figs. 4, 7 and 8 and A-1 similar to the salt concentration profile in Fig. 5. The mass transport limitations and corresponding salt concentration overpotential are discussed in detail later in this paper.

3.1.6. Charge transfer overpotential

The Butler Volmer form of expression is used in the simulations to describe the charge transfer kinetics. The average charge transfer overpotentials obtained from detailed simulations seen in the stacked plot in Fig. 4 are also shown in Fig. 9 during galvanostatic charging at 42.6 A m^{-2} (2C rate). The positive and the negative electrodes contributions approximately range between 80–100 mV and 120–140 mV respectively. If lithium plating were to occur, as this is shown to be thermodynamically possible in Fig. 3, the kinetics of this side reaction has to be included in the model and this can affect the performance predictions as mentioned before. In addition charge transfer overpotential could also be influenced by

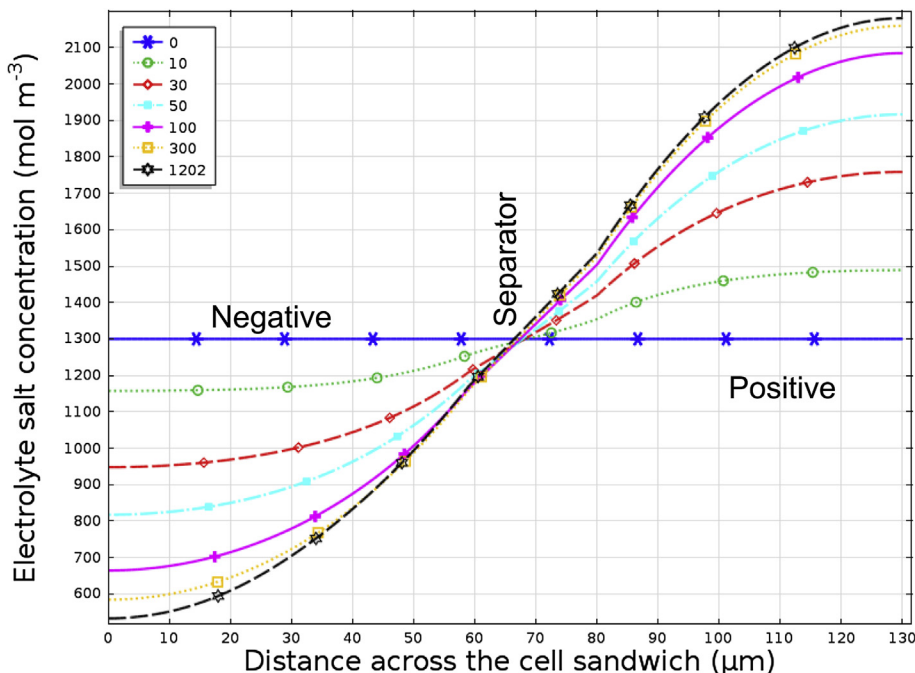


Fig. 5. Electrolyte (salt) concentration profiles across the cell sandwich at various times during galvanostatic charge at 42.6 A m^{-2} (2C rate). Legend is charge time in seconds.

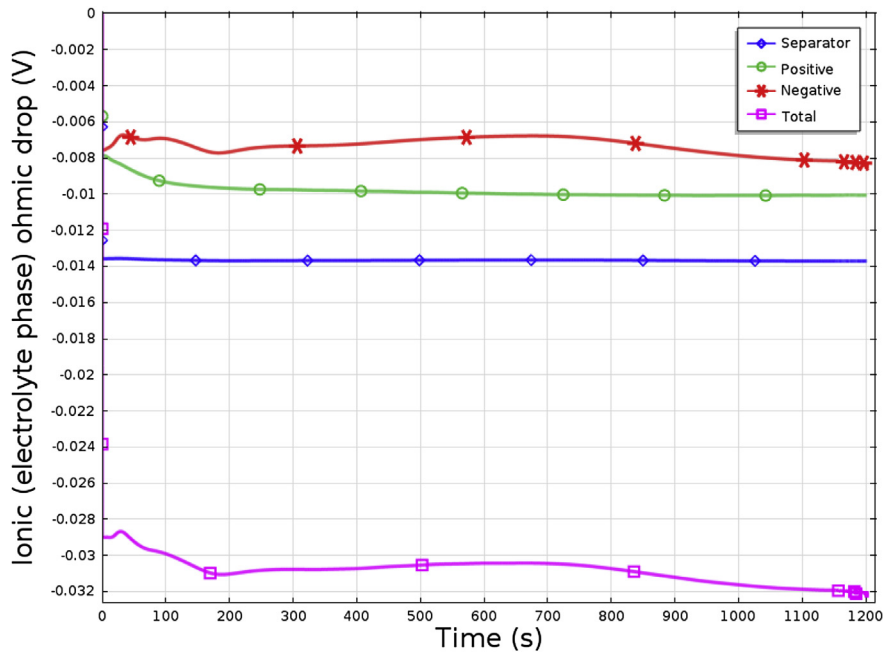


Fig. 6. Contributions to the ohmic potential drop in the liquid electrolyte (ionic) phase during galvanostatic charge at 42.6 A m^{-2} (2C rate) as a function of time. Liquid phase potential is taken to be measured with a lithium reference electrode.

solid phase diffusion limitations, as discussed later. Although the contribution of film resistance to the surface overpotential [2] and the possibility of its continuous increase with charge–discharge cycle are not explicitly considered in this work, the kinetic rate constants for the charge transfer reactions at the electrodes have been adjusted as in Table 1.

3.1.7. Mass transfer limitations and concentration overpotential in the electrolyte phase

The concentration overpotential in the electrolyte phase depends on salt concentration and its gradient in the cell and is

therefore affected by different transport properties, the thermodynamic factor that accounts for a non-ideal electrolyte as well as the porosity and tortuosity. Fig. 10 shows the concentration overpotential in the electrolyte phase from the simulation results for a 2C charge rate in each region of the cell which add up to approximately 43 mV (Fig. 4 and Fig. A-1). The negative electrode is the major contributor (Fig. 10), possibly due to the decreasing salt concentration in this region during charging (Fig. 5) as salt concentration is related to liquid phase potential drop through modified Ohm's law.

The time constant for diffusion in the electrolyte within the cell is roughly 240 s and the ratio of this time constant to that of the

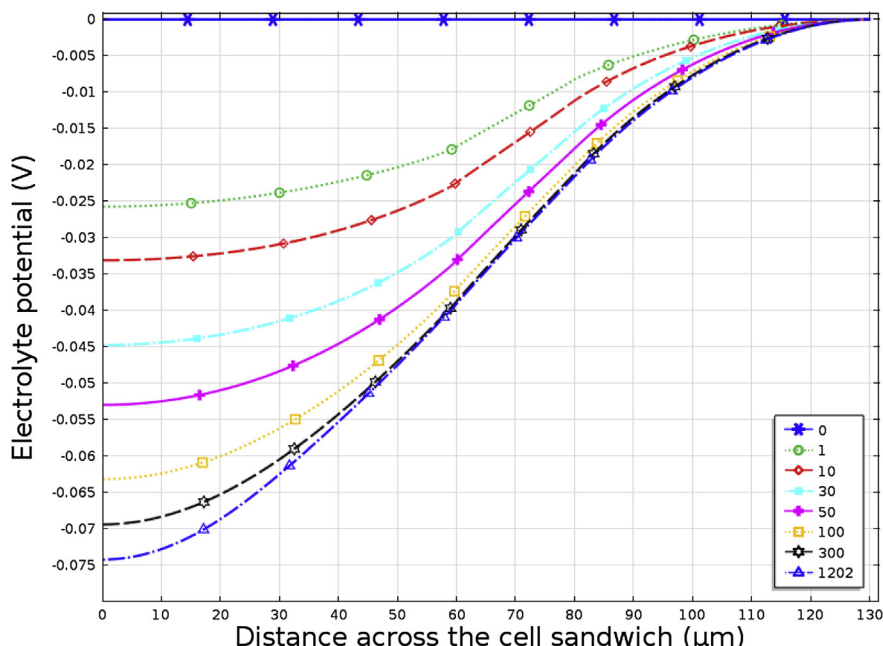


Fig. 7. Liquid electrolyte phase potential across the cell during galvanostatic charging at 42.6 A m^{-2} (2C rate). The electrolyte phase potential is taken to be measured with a lithium reference electrode and arbitrarily assumed to be zero at the positive-electrode/current-collector boundary. Legend is time in seconds.

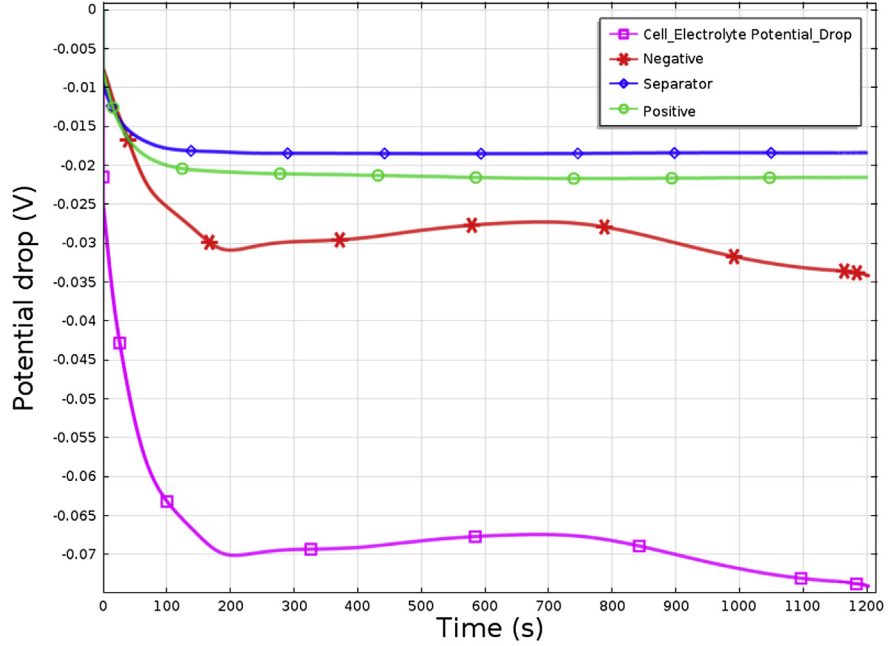


Fig. 8. Liquid electrolyte phase potential drop during constant-current charging at 42.6 A m^{-2} (2C rate) in each region and in the entire cell as a function of time.

charging time [10] at 2C is approximately 0.1 and is obtained using values in Table 1. Since the ratio is $<<1$, quasi steady-state concentration gradients will be quickly established compared to the charge time as seen in Fig. 5. This also explains the quasi steady-state profiles in Figs. 4, 7, 8 and 10 and A-1. It is clear from Figs. 1 and 5 that the cell cut-off potential is reached and charging stops long before the salt concentration can possibly hit zero at the negative electrode at 2C-rate. Likewise, the salt concentration does not reach the solubility limit at the positive electrode. All these confirm that although liquid phase mass transport overpotential contribute to the cell overpotential, other factors significantly influence the fast charging of this system at 2C.

3.1.8. Solid phase diffusion limitations

In considering lithium diffusion in the solid phase of the electrodes, the analysis here is limited to diffusion within spherical, secondary active material particles. Inter-particle diffusion, i.e. solid phase diffusion of lithium between particles in the electrode thickness direction is not considered. The time constants for lithium diffusion in the solid particles were calculated in an earlier work for this system [12] and are 2016 s in the negative and 35 s in the positive electrodes respectively. The ideal charge time at 2C rate is 1800 s. Therefore solid phase diffusion limitations occur in the negative electrode but are negligible in the positive. This is expected because the secondary active material particles at the

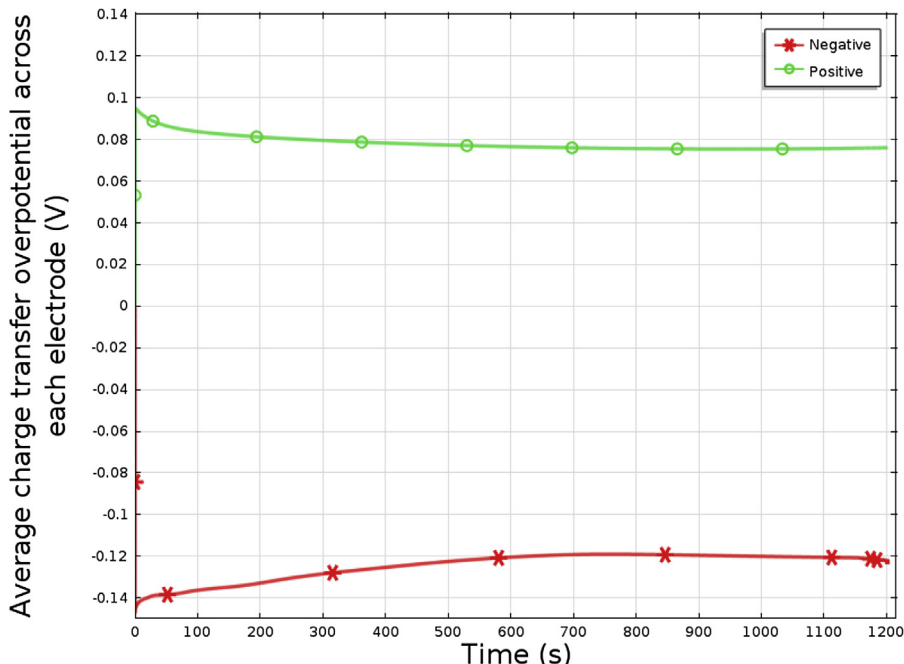


Fig. 9. Average charge transfer overpotential in each composite electrode while charging at 2C rate as a function of time.

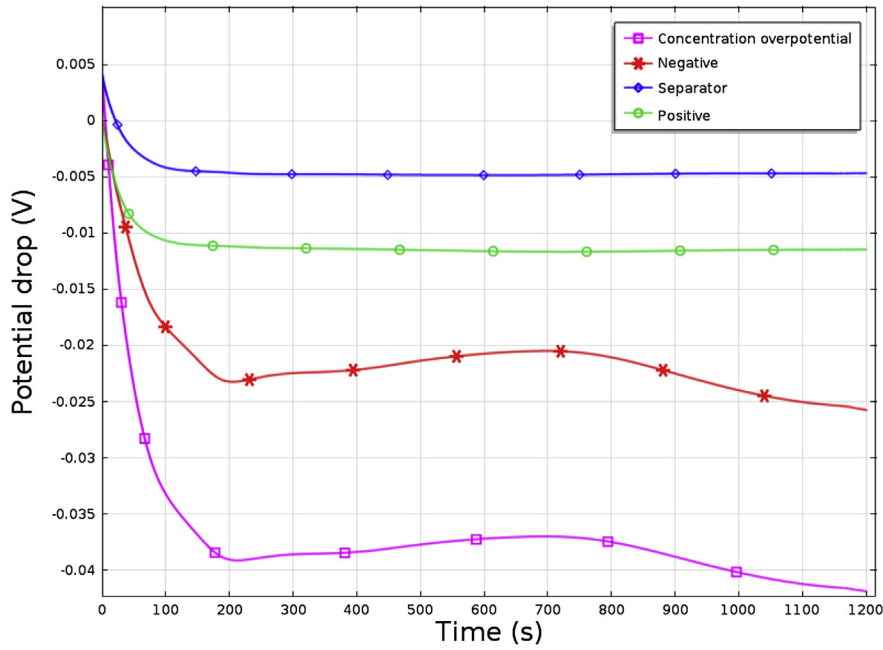


Fig. 10. Average electrolyte concentration overpotential as a function of time during charging at galvanostatic current density of 42.6 A m^{-2} .

negative electrode are bigger and the diffusion coefficient of lithium within the negative electrode particle is roughly one order of magnitude lower than that in the positive electrode.

Fig. 11 gives the solid lithium concentration within the secondary particles of negative electrode as a function of radial position at two different locations across the electrode thickness, namely, separator/electrode boundary and the current-collector/electrode boundary during galvanostatic charge at 2C. Irrespective of the location, there is a variation of Li concentration between the center and surface of the negative active material particle, verifying the quick estimates. Even though there is no concentration overpotential in the solid phase that is added directly to obtain the cell overpotential, the solid phase diffusion limitations are reflected in the cell overpotential through its influence on the lithium concentration at the surface of the particle across the cell sandwich (Fig. 12) and hence the charge transfer overpotential in two indirect ways as discussed in an earlier work [12]. Significant solid phase diffusion limitations at high rates of charging can increase the possibility of lithium plating on the negative electrode [2] that is shown to be thermodynamically feasible in Fig. 3. Fig. 12 implies the existence of a non-uniform reaction rate distribution across the thickness of the composite negative electrode (which influences Fig. 3 as well) and is examined next.

3.1.9. Local utilization across the cell sandwich

The local utilization of the active material (the average of the dimensionless solid Li concentrations at the surface and center of the particle) is plotted across each electrode in the cell sandwich direction in Fig. 13. The non-uniformity in local utilization (and hence the reaction rate distribution) increases in the negative electrode during the 2C charge. The reaction current distribution corresponding to the local utilization in Fig. 13 is also briefly described here. At short time (5 min), uniform current distribution prevails across the negative electrode and then the reaction front is skewed towards the negative-electrode/separator boundary. This distribution is then complicated with spans of spike-like front moving across the electrode thickness because of the strong influence of regions of flat thermodynamic open-circuit potential vs. composition curve

[10]. This effect is amplified by the potential difference of 0 V between the solid and liquid phase potentials in the composite electrode. An inflection or wave like pattern is seen in the surface lithium concentration at 900 s and 1100 s in the negative electrode in Fig. 12. Although quick estimatesⁱ suggest a local current density (in absolute values) of 2.35 Am^{-2} during charging at 2C rate, the non-uniform local current density varies up to a maximum of 4 A m^{-2} . As charging proceeds, the exchange current density becomes higher in regions closer to the negative-electrode/separator boundary than at the negative-electrode/current-collector boundary and is partly influenced by the local salt (Fig. 5) and solid lithium (Figs. 11 and 12) concentrations. The exchange current density ranges between 0.075 and 0.275 Am^{-2} in the negative electrode. Because of all the above reasons, surface overpotential at the negative electrode dominates the cell overpotential at 2C charge rate (Fig. 4).

Due to lack of solid phase diffusion limitations in the positive electrode particle, the utilization in Fig. 13 and surface Li concentration (Fig. 12) are almost the same across the positive electrode. The reaction front or local current density is slightly skewed towards the electrode/separator boundary due to the dominance of ohmic effects at short times in the positive electrode. However, at long times, the distribution and hence the utilization is mostly uniform as in Fig. 13. As 2C charging proceeds, the exchange current density becomes higher at the positive-electrode/current-collector boundary than at the positive-electrode/separator boundary possibly due to the influence of salt concentration effects and ranges between 0.375 and 0.6 A m^{-2} . However, the local current density (and utilization in Fig. 13) is almost uniform

ⁱ Local current density – neg_{quick estimate} = $\frac{\left(\frac{\text{Galvanostatic current density}}{\text{Thickness Negative electrode}} \right)}{\left(\frac{3 \times \text{Volume fraction}}{\text{Radius of the particle}} \right)_{\text{Negative electrode}}} = \frac{\left(\frac{42.6}{59.1 \times 10^{-6}} \right)}{\left(\frac{3 \times 0.65}{6.35 \times 10^{-6}} \right)} = 2.35 \text{ A m}^{-2}$.

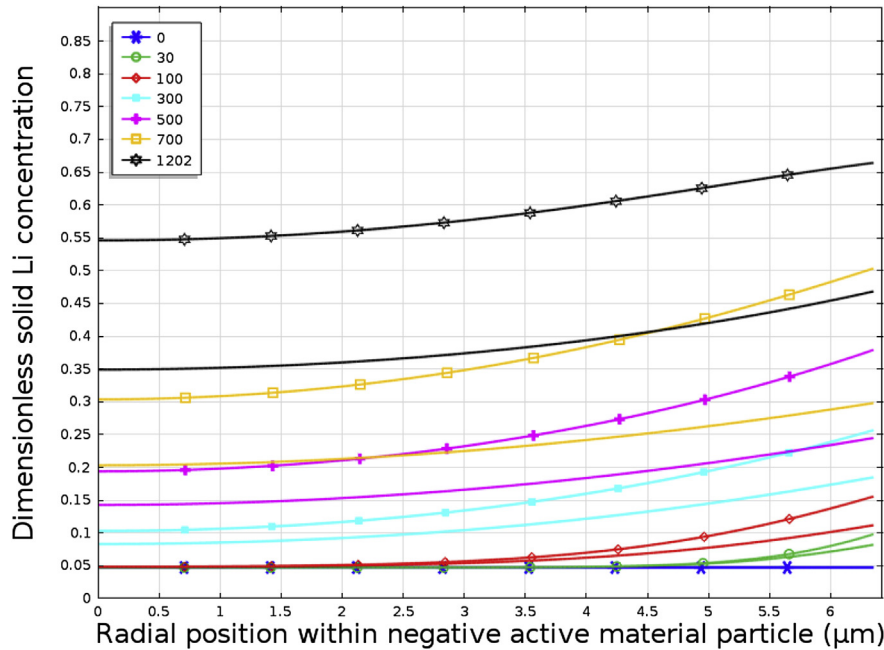


Fig. 11. Radial solid Li profile within secondary negative active material particle at 2C charge rate. Curves with markers: at electrode/separator boundary; no markers: at current collector/electrode boundary. Legend is charge time in seconds (same color is used for the curves at both the boundaries at any given time). (For interpretation of the references to color in this figure legend, the reader is referred to the web version of this article.)

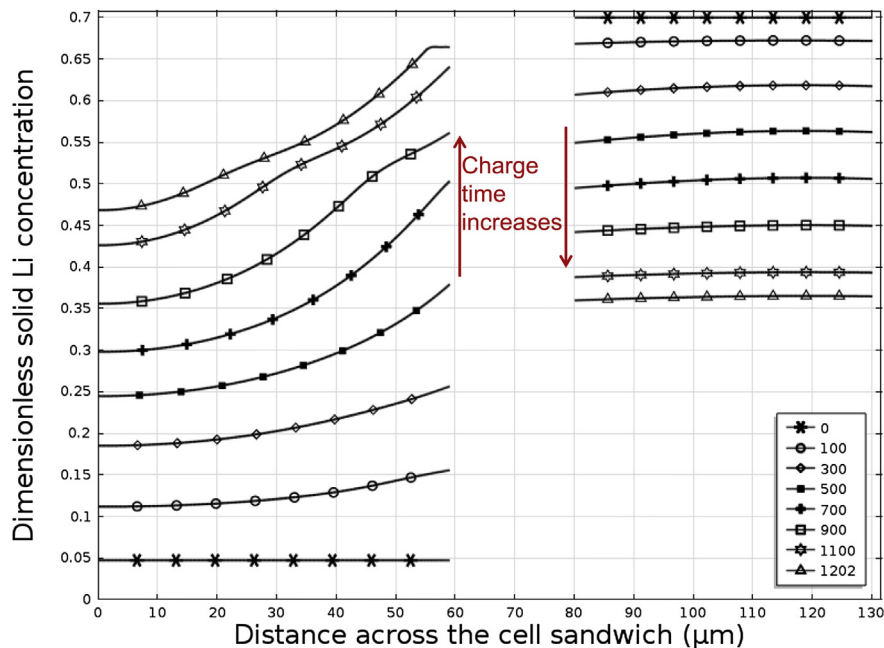


Fig. 12. Dimensionless solid lithium concentration profile at the surface of the active material particle across cell sandwich during charging at 2C (42.6 A m^{-2}). Legend is charge time in seconds.

($2.26\text{--}2.62 \text{ A m}^{-2}$ from simulations) and agrees with a quick estimateⁱⁱ of 2.35 A m^{-2} . This is because of the strong dependence of thermodynamic open-circuit potential on the lithium content in the positive electrode as well as the slow charge transfer kinetics

(Table 1). Significant contribution of the charge transfer kinetic limitations at the positive electrode to the cell overpotential is seen in Fig. 4.

3.2. Summary of individual contributions to the total overpotential in the cell

The contributions (in percentages) of the various processes from different regions of the cell to the total cell overpotential of 279 mV

ⁱⁱ Local current density – pos_{quick estimate} = $\frac{\left(\frac{42.6}{50 \cdot 10^{-6}}\right)}{\left(\frac{3.062}{5.15 \cdot 10^{-6}}\right)} = 2.35 \text{ A m}^{-2}$.

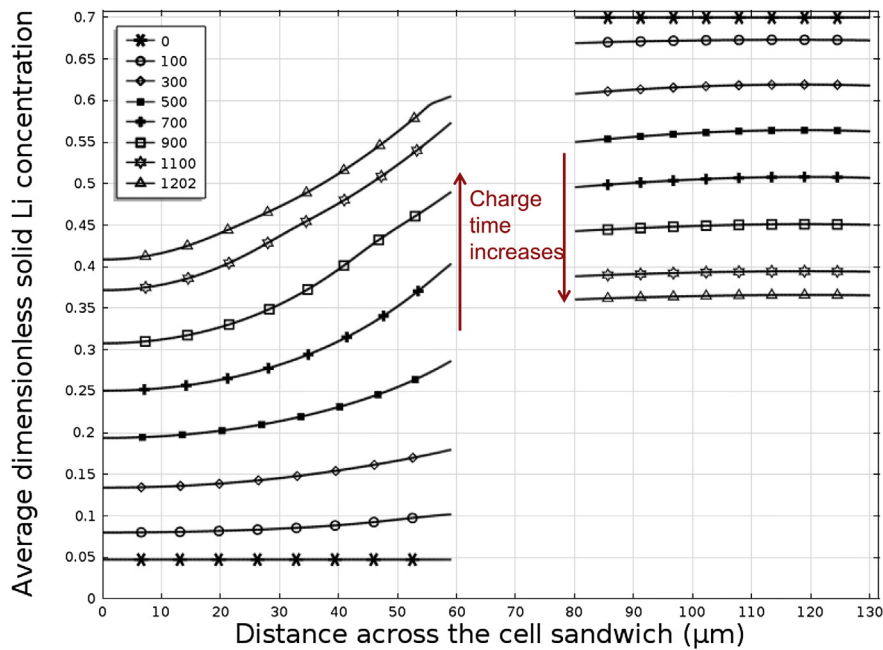


Fig. 13. Local utilization of active material in the composite electrodes during charge at 2C rate. Legend is charge time in seconds.

at the end of galvanostatic charging at a current density of 42.6 A m^{-2} (2C) is given in a pie chart in Fig. 14. The dominant portion (93%) of the cell overpotential arises from contributions from the positive (36%) and negative (57%) composite porous electrodes and only 7% of the cell overpotential is accounted for by the separator at the end of 2C rate of charge. When broken down by the contributing process, at a 2C charge rate, 12% is due to the ohmic (ionic) overpotential in the electrolyte phase and 15% is due to the electrolyte salt concentration overpotential. Thus, the electrolyte phase contributes to roughly 27% of the total cell overpotential at 2C charge rate (and roughly 31% at 3C charge rate). The remainder (73%) of the cell overpotential is attributed to contributions from charge transfer overpotential in the electrodes. Solid phase diffusion limitations in the negative electrode influence other contributions such as the charge transfer overpotential and therefore are indirectly reflected in these charts (Figs. 4 and 14). As mentioned before, although film resistance and other contact resistances are not explicitly considered in this work, adjustments to kinetic rate constants as in Table 1 have been made and hence their

influence on the cell overpotential has been indirectly captured in this work. To enable better charge acceptance during fast charging, the various overpotentials must be reduced to the extent possible. Furthermore, it is shown (Fig. 3) in this work that lithium plating is thermodynamically feasible during fast charging at 2C and beyond for this system. Eliminating some of the limitations will not only reduce the corresponding overpotentials shown in Figs. 4 and 14, but may also either delay or eliminate the possibility of lithium plating. However, it is prudent to take additional steps to ensure that lithium plating does not occur at all for safety reasons.

4. Conclusions

The simulation results from an isothermal physics-based dual lithium-ion insertion cell sandwich model are validated with experimental data at various constant-current charge rates. This paper has quantitatively shown that there are significant cell sandwich level bottlenecks to charging lithium-ion batteries at faster rates because the cell overpotential is higher at higher charge current density. Simulation results show that the cell can be charged only to 67% and 57% of the designed capacity at 2C and 3C constant-current rates (without a subsequent constant-voltage step) respectively due to corresponding overpotential losses of 279 and 414 mV. Solid phase diffusion limitation in the negative electrode, charge transfer overpotential, electrolyte concentration overpotential and ohmic (ionic) overpotential influence the charge acceptance for the cell design and operating conditions chosen in this work. Most important, it has been shown that lithium plating is thermodynamically feasible during charging at 2C rate and beyond which poses a challenge to battery safety in the long run. Additional experiments including teardown analysis may be needed to confirm if lithium plating actually occurs. Experimental work is also needed to quantify the contribution from interfacial film resistance and other electronic contact resistances and these can also lead to further adjustment of the kinetic rate constants.

The analyses in this paper are applicable to the particular chemistries, electrode design parameters and operational conditions described. Additives for safety, good solid electrolyte

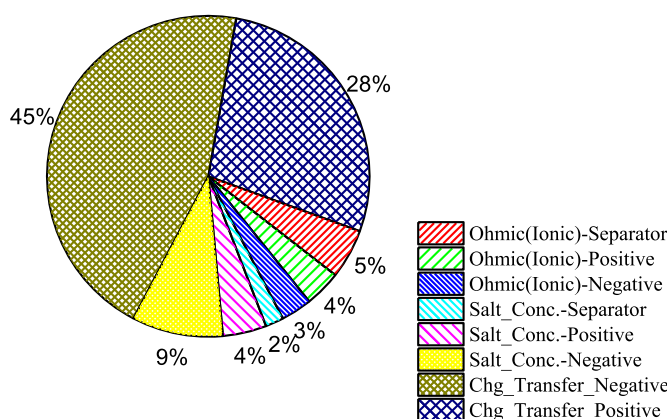


Fig. 14. Contributions to the cell overpotential (279 mV) at the end of galvanostatic charging at 2C rate (42.6 A m^{-2}).

interphase (SEI) formation, etc. are frequently used in commercial lithium-ion cells which are not considered in this model. Methods to reduce or eliminate the limitations (and associated overpotential) discussed in this work include enhancing the bulk and surface properties to enable fast charge acceptance. Furthermore, alternate positive (e.g. $\text{LiNi}_{0.8}\text{Co}_{0.15}\text{Al}_{0.05}\text{O}_2$ (i.e. NCA), lithium–manganese-rich layered oxides, etc.) and negative electrode active material chemistries may be used in lithium-ion cells for advanced electric vehicles. Therefore, the relative contributions

Acknowledgments

I extend my thanks to Andy Drews and Ted Miller from Ford Motor Company for their support. I thank the Samsung SDI team for the experimental data for prior works [11,14].

Appendix A

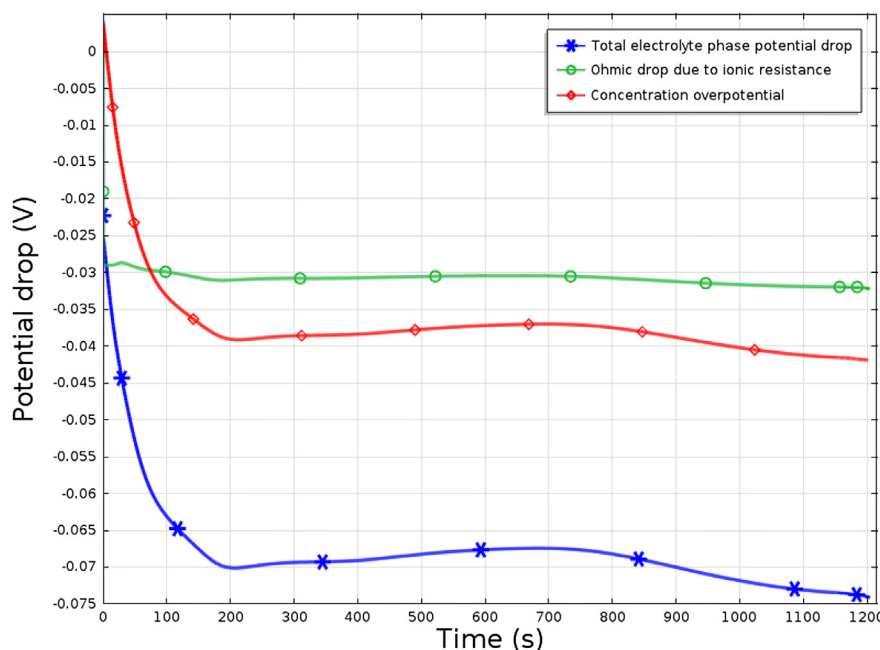


Fig. A-1. Contributions to the potential drop in the electrolyte phase as a function of time during galvanostatic charging at 42.6 A m^{-2} (2C).

from different components and the processes may vary from that discussed in this paper. However, the framework discussed in this work can be used to analyze bottlenecks to fast charging in other systems as well. Sometimes, modifications such as inclusion of thermodynamic open-circuit voltage fade for lithium–manganese-rich layered oxides or volume changes for silicon negative electrodes are necessary.

Simulations in this work are based on the cell sandwich model and so while extending these analyses to large format cells, non-uniform current distributions across the cell geometries have to be considered [12]. Fast charging can heat up the cell and lead to a non-uniform temperature distribution. The electrodes and cell components may also be mechanically stressed due to repeated high rate charge–discharge cycles. A 3D-electrochemical-thermal-mechanical-life model is needed to more accurately predict the fast charge performance of lithium-ion cells in advance electric vehicles, driven in different regions with varied temperature conditions. This work is significant because it provides a framework and quantitatively identifies the issues that challenge fast charging of advance electric vehicle batteries.

References

- [1] R. Chandrasekaran, ECS Trans. 58 (48) (2014) 121–144.
- [2] M. Doyle, J.S. Newman, A.S. Gozdz, C.N. Schmutz, Jean-Marie Tarascon, J. Electrochem. Soc. 143 (1996) 1890–1903.
- [3] US DOE Vehicle Battery R&D: Progress Update, David Howell et al.
- [4] G. Sikha, P. Ramadass, B.S. Haran, R.E. White, B.N. Popov, J. Power Sources 122 (2003) 67–76.
- [5] P. Ramadass, B. Haran, R.E. White, B.N. Popov, J. Power Sources 111 (2002) 210–220.
- [6] H. Zhang, X. Yu, P.V. Braun, Nat. Nanotechnol. 6 (2011) 277–281.
- [7] B. Kang, G. Ceder, Nature 458 (2009) 190–193.
- [8] K. Zaghib, J.B. Goodenough, A. Mauger, C. Julien, J. Power Sources 194 (2009) 1021–1023.
- [9] G. Ceder, B. Kang, J. Power Sources 194 (2009) 1024–1028.
- [10] T.F. Fuller, M. Doyle, J.S. Newman, J. Electrochem. Soc. 141 (1994) 1–10.
- [11] R. Chandrasekaran, Y. Seong, C. Bae, J. Jung, K. Kim, K. Cheong, T.J. Miller, Mater. Res. Soc. Online Proc. Libr. (2013). MRS13-1541-F04-05.
- [12] R. Chandrasekaran, J. Power Sources 262 (2014) 501–513.
- [13] T. Ohzuku, Y. Iwakoshi, K. Sawai, J. Electrochem. Soc. 140 (9) (1993) 2490–2498.
- [14] R. Chandrasekaran, C. Bae, Y. Seong, T.J. Miller, Publication # 81, in: 248th ACS National Meeting, 2014, http://abstracts.acs.org/chem/248nm/program/view.php?obj_id=282351&terms=.
- [15] M. Doyle, T.F. Fuller, J.S. Newman, J. Electrochem. Soc. 140 (1993) 1526–1533.
- [16] P. Arora, R.E. White, J. Electrochem. Soc. 145 (10) (1998) 3647–3667.